Electronic Supporting Information

Opto-magnetic optimization enhances multimodal therapeutic and diagnostic (UCL/T_1-T_2W MRI) potentialities of GdOF against MDA-MB-231

Tanmoy Mondal[†,a], Panchanan Sahoo[†,a], Sourav Kumar Nandi[a], Sudip Kundu[a], Menglong Li[b], Nibedita Haldar[a], Raushan Kabir[a], Koushik Mitra[c], Shubham Roy[d], Mandira Das[a] and Chandan Kumar Ghosh*[,a]

Author affiliation

[a] School of Materials Science and Nanotechnology, Jadavpur University, Kolkata-700032, India

[b] Shenzhen Nanshan People's Hospital (NSPH), 89 Taoyuan Road, Nanshan District, Shenzhen 518052, China

[c] Department of Industrial Chemistry & Applied Chemistry, Swami Vivekananda Research Centre, Ramakrishna Mission Vidyamandira, Belur Math, Howrah, India

[d] School of Science, Harbin Institute of Technology, Shenzhen, Guangdong 518055, China

[†] T. Mondal and P. Sahoo have equally contributed in this work.

* Corresponding author

E-mail: chandu_ju@yahoo.co.in

Table S1: Unit cell parameters of YEGdOF samples as obtained from Reitveld analysis

Properties		**$Y_{0.1}E_{0.01}GdOF$**	**$Y_{0.1}E_{0.03}GdOF$**	**$Y_{0.1}E_{0.05}GdOF$**	**$Y_{0.1}E_{0.07}GdOF$**
Lattice parameter (A^0)	**a=b**	3.857(4)	3.847(4)	3.838(3)	3.830(2)
	c	19.244(6)	19.195(3)	19.189(6)	19.122(9)
Unit cell volume ($(A^0)^3$		247.974(18)	246.107(16)	244.910(7)	243.040(18)
Bond length (A^0)	**Gd-O**	2.486(6)	2.480(10)	2.475(2)	2.469(11)
	Gd-F	2.610(9)	2.598(7)	2.568(3)	2.562(16)
Bond angle (in degree)	**Gd-O-Gd**	116.182(11)	116.179(5)	116.226(4)	116.193(13)
	F-Gd-O	82.130(12)	82.049(3)	82.390(12)	82.118(19)
	F-Gd-F	96.265(16)	96.355(10)	96.177(12)	96.225(20)
	O-Gd-O	63.615(14)	63.618(7)	63.571(16)	63.605(18)
	Gd-F-Gd	120.227(16)	120.158(8)	120.276(17)	120.240(16)
Strain (%)		0.25(4)	0.32(3)	0.42(2)	0.48(1)
Crystallite size (nm)		14.1(20)	17.2(30)	18.5(15)	23.2(16)
R_p (%)		15.00	12.31	16.20	14.46
R_{wp} (%)		17.90	16.20	14.50	15.20
R_{exp} (%)		14.30	11.50	12.30	13.30
χ^2		1.46	1.06	1.18	1.16

Table S2: TCSPC experimental values of the parameter A_1, A_2, τ_1, τ_2 and τ_{avg}

Samples (λ_{ex} = 654 nm)	τ_1 **(ms)**	τ_2 **(ms)**	A_1	A_2	τ_{avg} **(µs)**
$Y_{0.1}E_{0.01}GdOF$	0.14189	0.0291	4.37409	89.55451	51
$Y_{0.1}E_{0.03}GdOF$	0.01482	0.08815	1.11462	0.15979	48
$Y_{0.1}E_{0.05}GdOF$	0.0301	0.26859	0.94888	0.01252	28
$Y_{0.1}E_{0.05}GdOF$	0.33338	0.04907	0.03703	0.91625	11

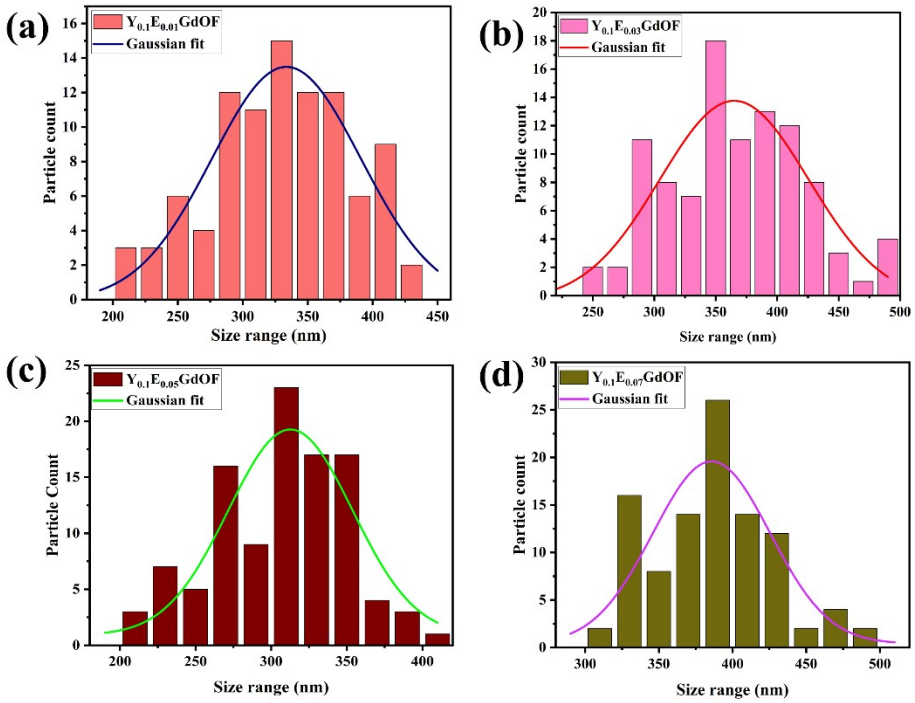

Figure S1: Histogram of the particle size distribution of (a) $Y_{0.1}E_{0.01}GdOF$, (b) $Y_{0.1}E_{0.03}GdOF$, (c) $Y_{0.1}E_{0.05}GdOF$, and (d) $Y_{0.1}E_{0.07}GdOF$ samples.

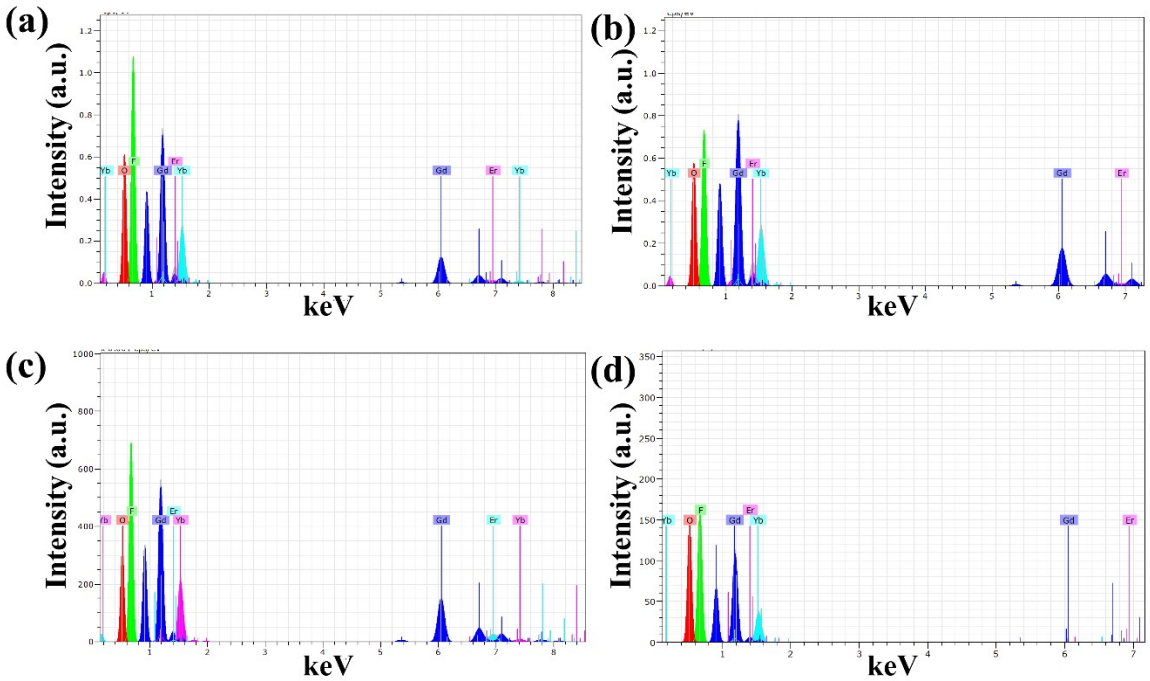

Figure S2: EDX spectra of (a) $Y_{0.1}E_{0.01}GdOF$, (b) $Y_{0.1}E_{0.03}GdOF$, (c) $Y_{0.1}E_{0.05}GdOF$, and (d) $Y_{0.1}E_{0.07}GdOF$ samples.

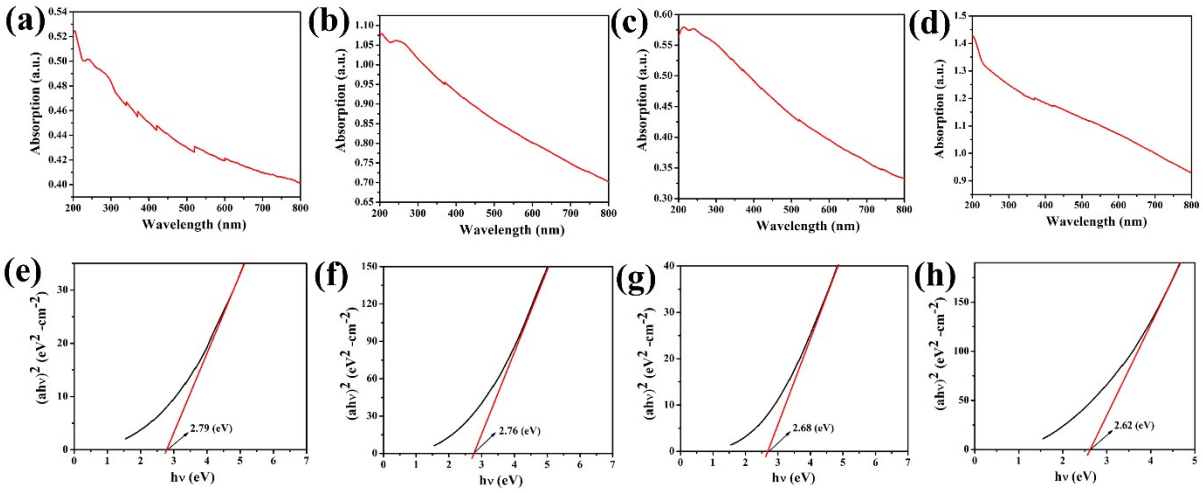

Figure S3: Uv-Vis absorption spectra and corresponding band gap of (a, e) $Y_{0.1}E_{0.01}GdOF$, (b, f) $Y_{0.1}E_{0.03}GdOF$, (c, g) $Y_{0.1}E_{0.05}GdOF$ and (d, h) $Y_{0.1}E_{0.01}GdOF$ samples.

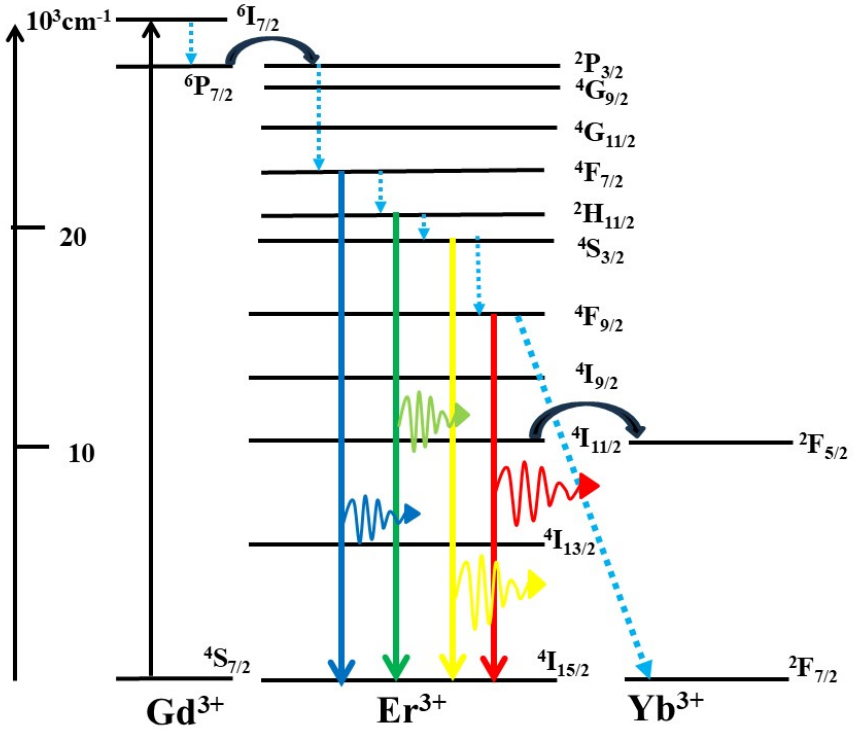

Figure S4: Down conversion transition energy diagram YEGdOF samples.

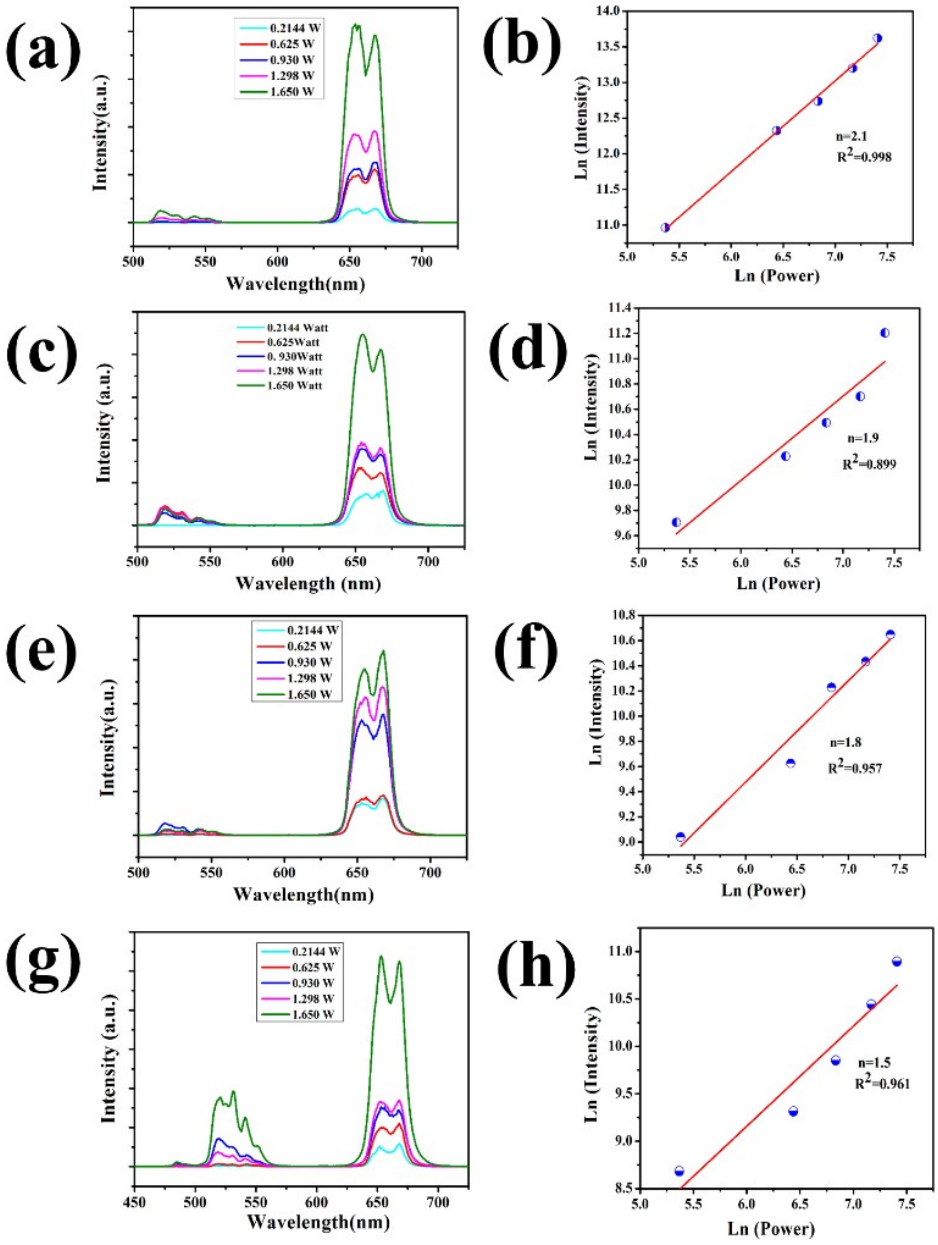

Figure S5: Upconversion photoluminescence spectrum at various power and Pump power density dependence of the red upconversion luminescent intensity of the (a,b) $Y_{0.1}E_{0.01}GdOF$; (c,d) $Y_{0.1}E_{0.03}GdOF$; (e, f) $Y_{0.1}E_{0.05}GdOF$; and (g, h) $Y_{0.1}E_{0.01}GdOF$ samples respectively.

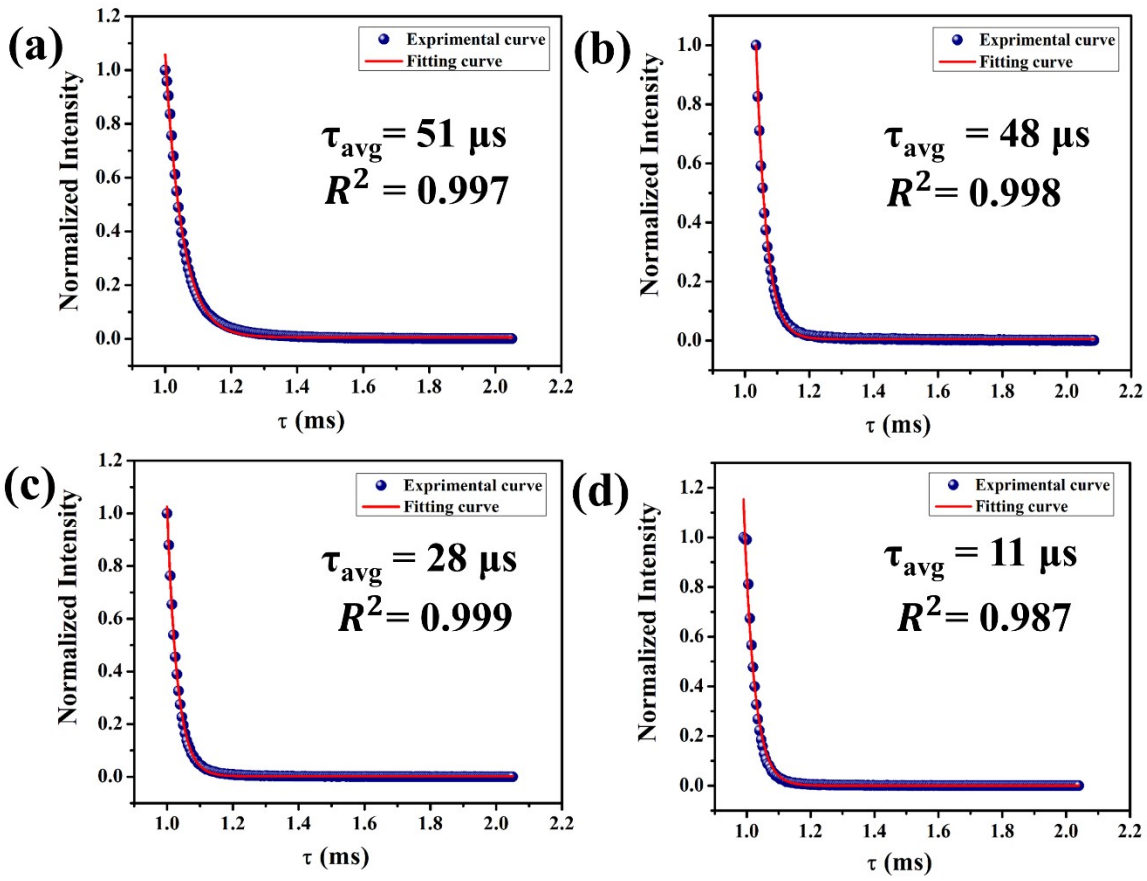

Figure S6. Time average decay profile of YEGdOF samples: (a) $Y_{0.1}E_{0.01}GdOF$, (b) $Y_{0.1}E_{0.03}GdOF$, (c) $Y_{0.1}E_{0.05}GdOF$, and (d) $Y_{0.1}E_{0.07}GdOF$ samples. λ_{ex} = 980 nm and λ_{em} = 655 nm.

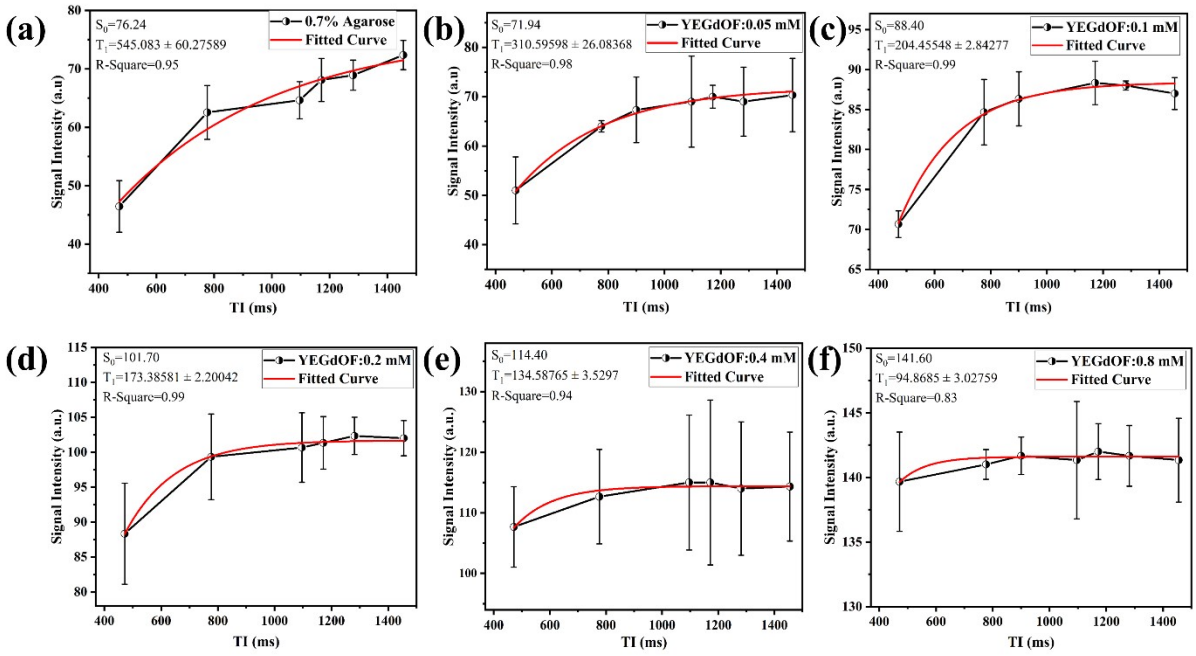

Figure S7: Longitudinal signal intensity vs inversion time plot as a function of $Y_{0.1}E_{0.01}GdOF$ concentration, (a) 0.7% Agarose, (b) 0.05 mM, (c) 0.1 mM, (d) 0.2 mM, (e) 0.4 mM and (f) 0.8 mM.

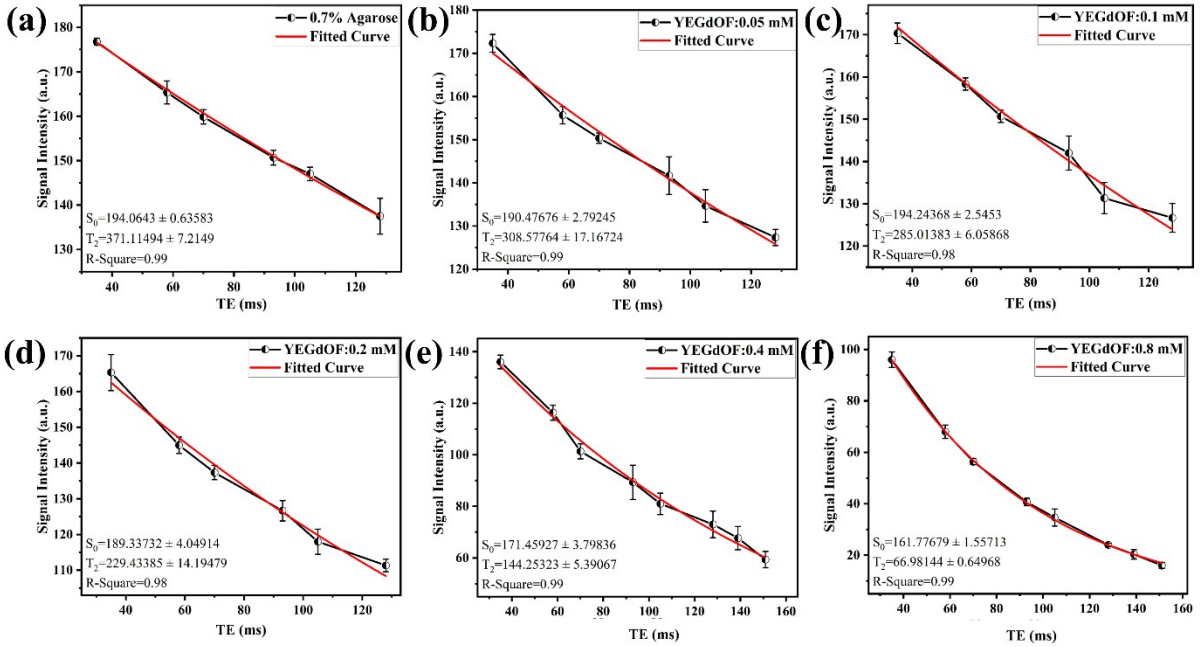

Figure S8: Transverse signal intensity Vs echo time plot as a function of $Y_{0.1}E_{0.01}GdOF$ concentration, (a) 0.7% Agarose, (b) 0.05 mM, (c) 0.1 mM, (d) 0.2 mM, (e) 0.4 mM and (f) 0.8 mM.

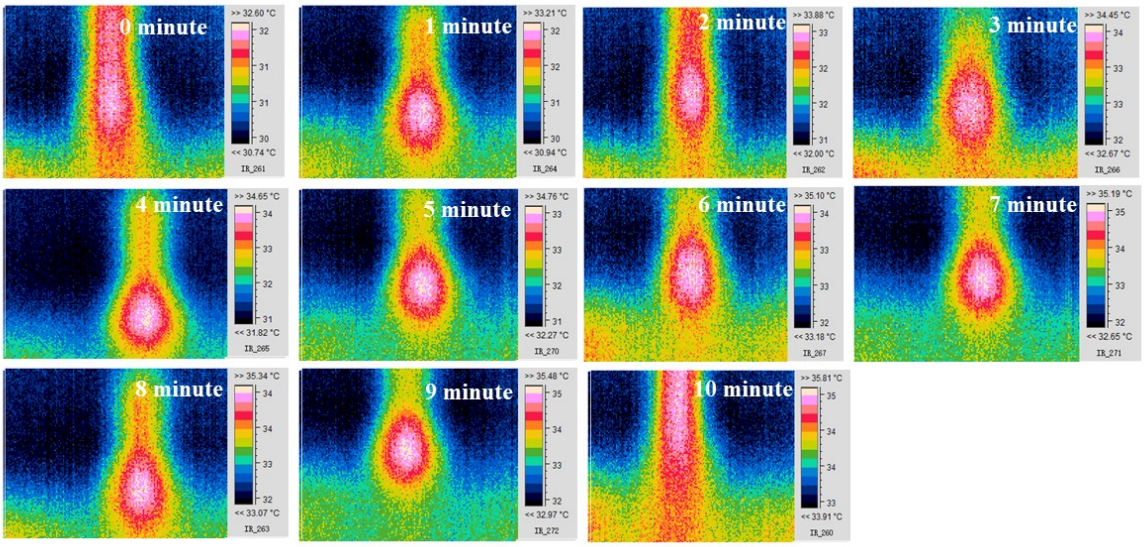

Figure S9: Photothermal images of Deionized water under continuous NIR laser (980 nm) exposure for 10 minute.

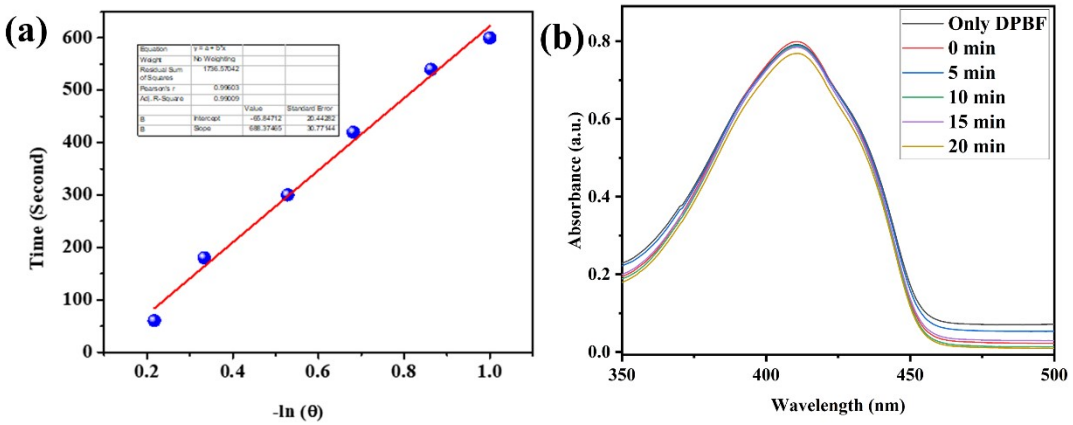

Figure S10: (a) Linear fit for time versus negative natural logarithmic temperature increase for cooling rate of $Y_{0.1}E_{0.01}GdOF$. (b) UV−Vis absorption spectra for the time dependent degradation of DPBF by pristine $Y_{0.1}E0_{.01}GdOF$ sample under dark condition, showing no significant change in absorbance of DPBF.

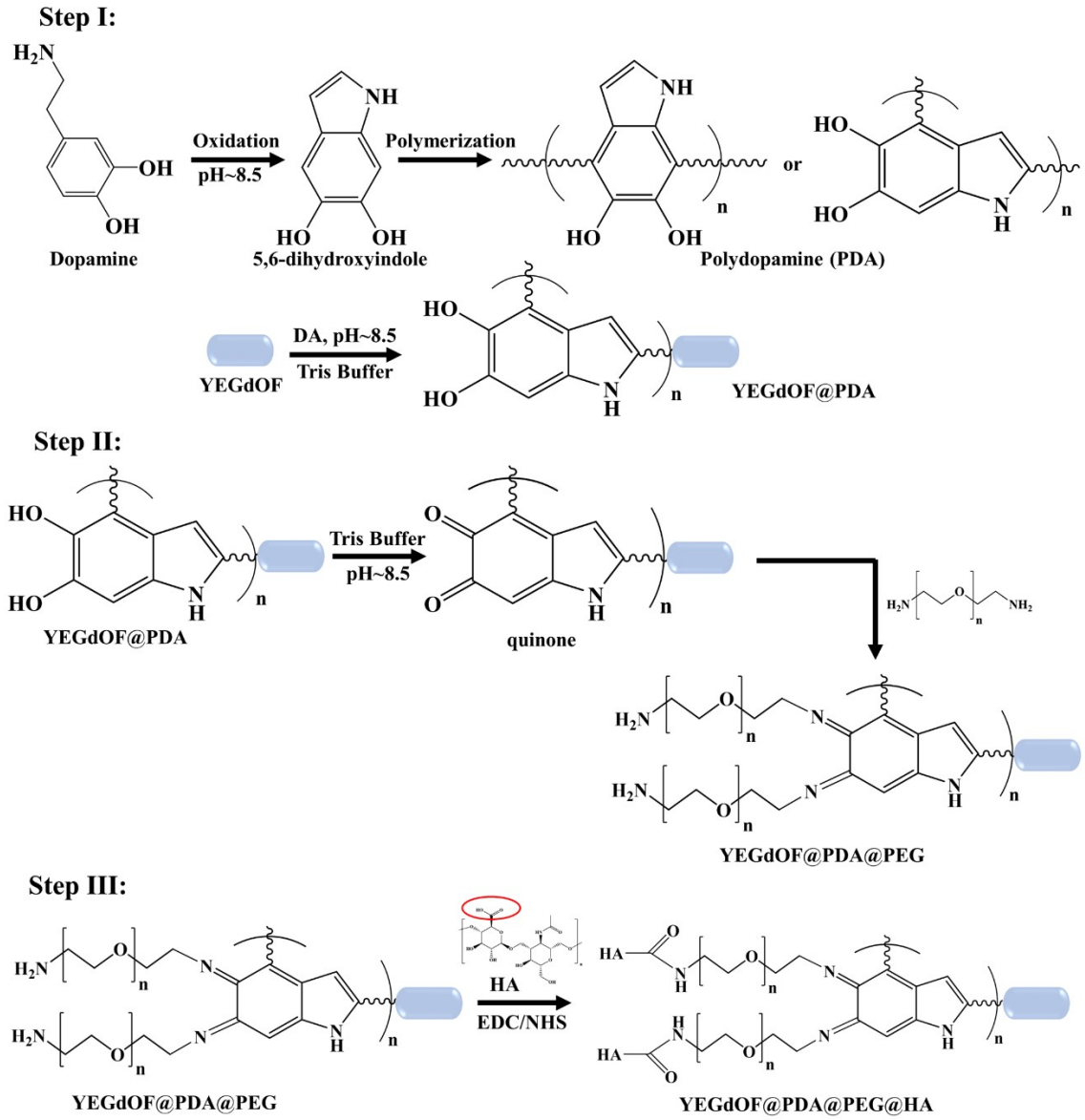

Figure S11: Schematic representation of probable synthesis mechanism of individual step of functionalization step, showing key chemical structure and nature of bonds.

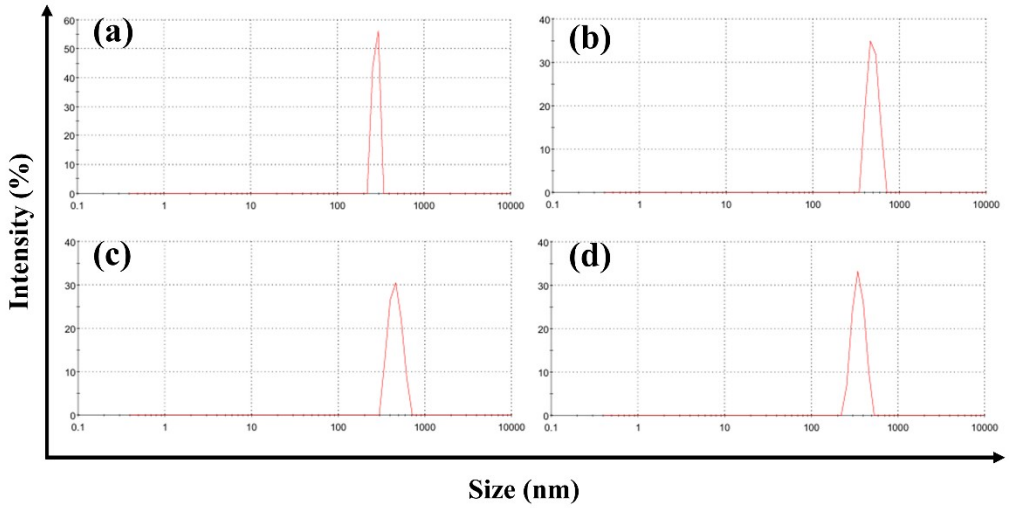

Figure S12: DLS measurement of individual step of surface modifications. (a) Bare $Y_{0.1}E_{0.01}$GdOF; (b) $Y_{0.1}E_{0.01}$GdOF@PDA; (c) $Y_{0.1}E_{0.01}$GdOF@PDA@PEG; (d) $Y_{0.1}E_{0.01}$GdOF@PDA@PEG@HA@DOX.

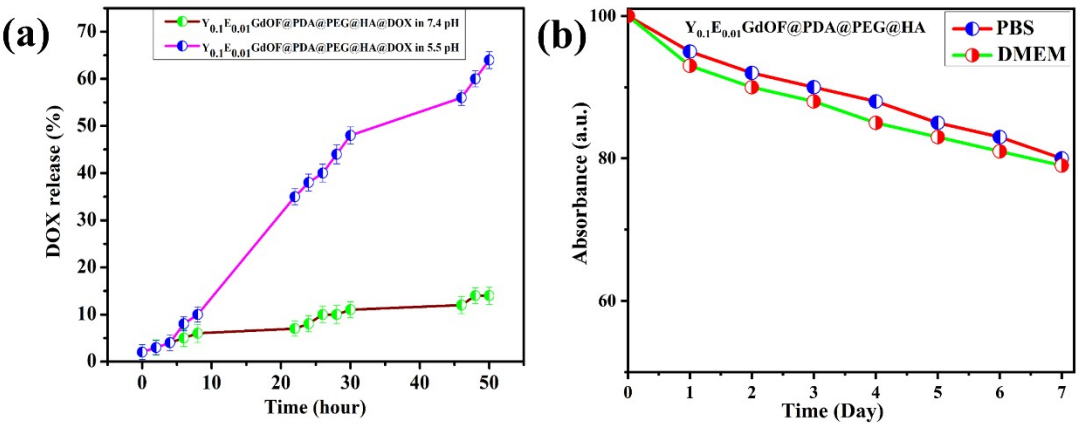

Figure S13: (a) pH dependant DOX releasing profile. (b) Time dependant stability plot in PBS (pH~ 7.4) and DMEM (pH~ 5.5).

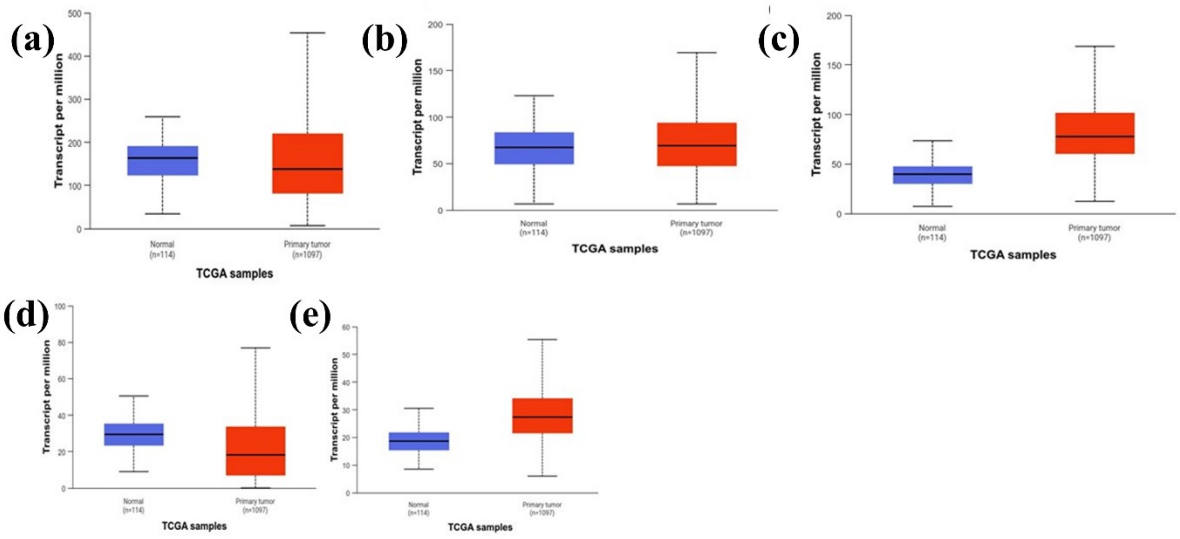

Figure S14: Expression of CD44 (a); TP53 (b); BAX (c); BCL-2 (d); and CASP-3 (e) in normal and tumor from TCGA samples.

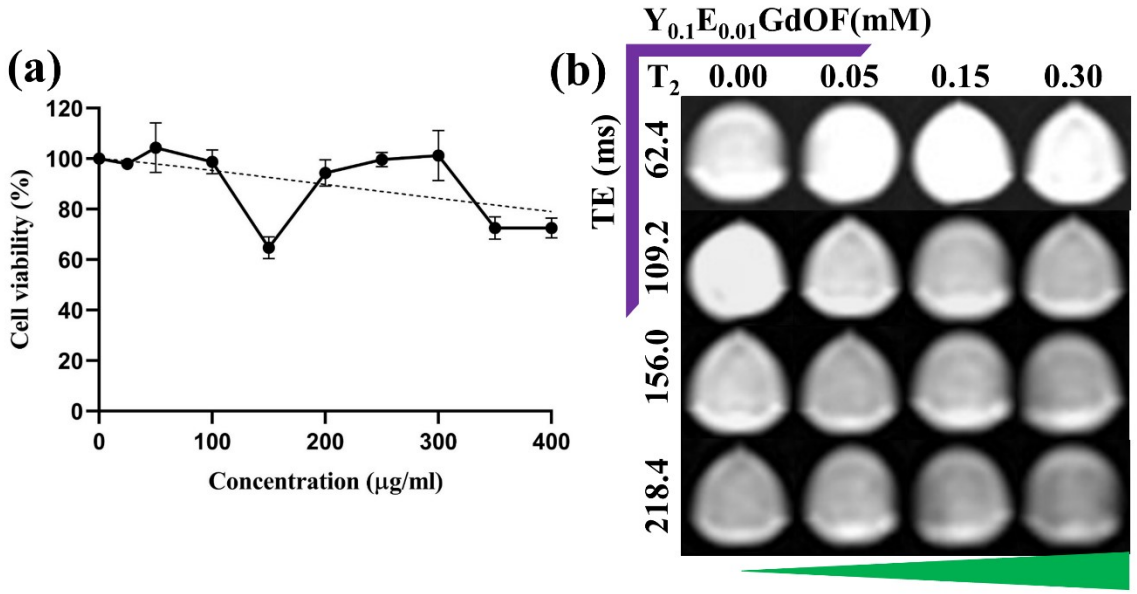

Figure S15: Concentration-dependent (a) cell viability; (b) T_2W cellular MR phantom images observed for $Y_{0.1}E_{0.01}$GdOF@PDA@PEG@HA@DOX treated WI 38.